Stability Analysis of Grid-Connected VSC Dominated by PLL Using Electrical Torque Method

Xiaofang Wu, Zhengchun Du, *Senior Member, IEEE*, Yujun Li, *Member, IEEE*, and Xiaotian Yuan, *Graduate Student Member, IEEE*

***Abstract*—The instability issue of the grid-connected Voltage Source Converter (VSC) dominated by phase-lock loop (PLL) is investigated using the electrical torque method in this paper. The system dynamic model and steady-state relationship of variables are first established. Then, a basic two-order model representing the PLL natural oscillation mode is extracted. The impacts of the current control loop and altering current grid (ACG) on the PLL oscillation mode are derived using the electrical torque method. As a result, analytical expressions of the system synchronous and damping coefficients are obtained. Based on the derived synchronous and damping coefficient, qualitative evaluations of the impacts of the system parameters on the oscillation frequency and system stability can be achieved. It is drawn that a small PLL time constant, low infinite source voltage, heavy load, reactive power absorption, and long electrical distance will deteriorate system stability. Moreover, a sufficient analytical stability criterion for the grid-connected VSC is derived from the damping coefficient. The system stability can be directly evaluated through the operation points and system parameters, and the quantitative evaluation of the system stability is achieved. The eigenvalue analysis and electromagnetic transient simulation have verified the reliability and effectiveness of the theoretical analysis.**

***Index Terms*—Stability analysis, phase-locked loop (PLL), voltage source converter (VSC), electrical torque method, synchronous and damping coefficients, stability criterion.**

NOMENCLATURE

$\boldsymbol{u}_c$	Converter output voltage.
$\boldsymbol{u}_p$	PCC voltage.
$\boldsymbol{i}_{pr}$	Current across the converter.
$\boldsymbol{u}_s$	Infinite source voltage.
ω_s	System angular speed.
ω	PLL measured angular speed.
x_1	Integrator variable of PLL.
θ	The angle the *d-axis* leading $\boldsymbol{u}_s$ with.
x_2 andx_3	*d/q*-axis integrator variables of the inner current controller.
$P_c$and Q_c	Active and reactive transmitted power.
Superscripts "*d*" and "*q*"	*d/q* components of variables.
Superscripts "*ref*"	Reference of the inner current controller.
Superscripts "(0)"	Steady-state value of variables.

Manuscript received 31 August 2021; revised 9 January 2022; accepted 27 February 2022. Date of publication 3 March 2022; date of current version 22 August 2022. This work was supported by the National Natural Science Foundation of China under Grants U2066602 and 51807150. Paper no. TEC-00936-2021. *(Corresponding author: Yujun Li.)*

Xiaofang Wu, Zhengchun Du, and Yujun Li are with the School of Electrical Engineering, Xi'an Jiaotong University, Xi'an 710049, China (e-mail: xiaofangwu@stu.xjtu.edu.cn; zcdu@xjtu.edu.cn; yujunlizju@gmail.com).

Xiaotian Yuan is with the School of Electrical Engineering, Xi'an Jiaotong University, Xi'an 710049, China, and also with the School of Electrical and Electronic Engineering, Nanyang Technological University, Singapore 639798 (e-mail: yxt2013@stu.xjtu.edu.cn).

Color versions of one or more figures in this article are available at https://doi.org/10.1109/TEC.2022.3156054.

Digital Object Identifier 10.1109/TEC.2022.3156054

I. INTRODUCTION

POWER electrical equipment is widely used in modern power system generation, transmission, and other related fields. Increasing wind power and solar power generation facilities are integrated into power systems to relieve the pressure of fossil energy shortage [1]–[3]. Due to the advantages of no commutation failure, fewer current harmonics, and independent control of active and reactive power, VSC-HVDC and flexible ac transmission are widely used for long-distance power delivery [4]–[6]. As necessary components to connect electrical power elements and AC grid, voltage source converters (VSCs) play an essential role in modern power systems [7]–[9]. Their dynamic behaviors need further investigation when connecting a weak grid.

Some studies have been conducted on the stability analysis of grid-connected VSCs, and the most commonly used methods are the eigenvalue analysis method [10]–[13] and the impedance-based method [14]–[18]. In [10], the eigenvalue analysis is conducted based on the linearized model of the converter system, and the system stability is judged based on the real part of the eigenvalues. It is found that the dominated mode of the system is strongly related to the PLL control loop and the AC grid strength via the participation factors analysis [11], [12]. Moreover, the rough boundary of the maximum power transfer capability of the VSC can be derived via eigenvalue analysis [13]. Nevertheless, the eigenvalue analysis method depends on complex eigenvalue computation, which is time-consuming and needs to recompute once the system topology changes.

Another method, namely the impendence-based analysis method, is further proposed to study the stability of grid-connected VSC [14]. A VSC grid-connected system can be equivalent to a voltage source in series with a source impedance and a grid impedance, and then the system stability can be determined through the Nyquist criterion [15]. The multi-input and multi-output (MIMO) impedance model of the studied system

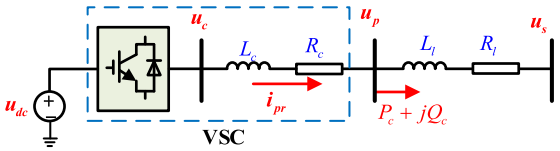

Fig. 1. Topology of a single VSC connected to an infinite bus through a transmission line.

is derived based on the small-signal model [16], [17], and it is found that the instability results from the negative resistance behavior of grid-tied inverters. Furthermore, using the impedance model of VSC, the multiple VSCs interfaced system can be simplified as RLC equivalent circuit to quantify the start-oscillating condition intuitively [18]. Using the eigenvalue analysis method and the impedance analysis method, the instability phenomenon of the grid-connected VSC can be comprehensively studied, and the influence factors are also confirmed. However, it is challenging to obtain neither the mechanism of insufficiency of damping nor the frequency characteristic of oscillation via the above two methods.

To study the insight mechanism of the instability phenomenon of the grid-connected VSC, the complex torque method is employed [21]–[23], which is widely used to investigate the frequency and damping characteristics of the traditional power grid [19], [20]. Through this method, PLL is modeled as a two-order model similar to the synchronous generator's rotor motion. The dynamics of the current control loop and ACG can be transformed as the additional damping coefficient on the PLL model [22]. Thus, the small signal stability can be easily judged by the sign of the damping coefficient. The high-order dynamic system is transformed into a two-order model to investigate its stability problem using the complex torque method, and the computational complexity is significantly reduced. Unfortunately, the damping and restoring coefficients obtained from the above studies are not in the analytical forms, failing to intuitively evaluate the impacts of system parameters on the dominated oscillation mode and establish an analytical stability criterion. In addition, they lack a discussion on the influencing factors of the oscillation frequency.

To overcome the deficiencies of the existing method, the electrical torque approach is proposed to investigate the small signal stability of the grid-connected VSC in this study. The analytical expressions of the synchronous and damping coefficients of the PLL oscillation mode are derived through the electrical torque method. Consequently, qualitative evaluations of the impacts of the operation conditions, the control parameters, and the system parameters on the dominated oscillation mode can be achieved. In addition, an analytical stability criterion for the grid-connected VSC is derived from the damping coefficient. Thus, the small-signal stability of the studied system under given operation conditions can be quantitatively evaluated.

To sum up, the main contributions of this paper are:

- The electrical torque method is applied to the linear model of the grid-connected VSC so that the analytical expressions of the synchronous and damping coefficients are obtained.
- Qualitative evaluations of the impacts of the system parameters on the oscillation frequency and system stability are conducted based on the derived synchronous and damping coefficients.
- An analytical stability criterion for the grid-connected VSC is derived from the analytical expression of the damping coefficient.

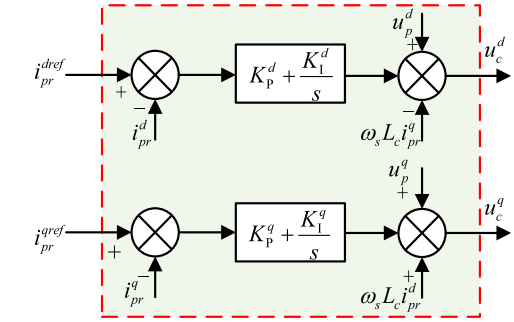

(a) Diagram of the inner current controller

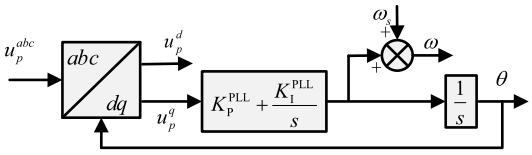

(b) Control block diagram of PLL

Fig. 2. Control system diagram.

II. The Grid-Connected VSC Model

A. System Model

Fig. 1 illustrates the topology of a single VSC connected to an infinite bus through a transmission line. The converter voltage is assumed to be three-phase symmetrical with no harmonic injection. In Fig. 1, R_c and L_c are the resistance and inductance of the phasor reactor, R_l and L_l represent the resistance and inductance of the transmission line. $\boldsymbol{u}_c$ and $\boldsymbol{u}_p$ are the voltage of the converter and point of common coupling (PCC). $\boldsymbol{i}_{pr}$ denotes the current across the converter. $\boldsymbol{u}_s$ denotes the voltage of the infinite source with the fixed system angular frequency marked as ω_s, fixed amplitude marked as U_s and the initial phase angle of zero.

The control system of the VSC consists of a phase-locked loop (PLL) and an inner current control loop, as shown in Fig. 2. The objective of the inner current controller is to keep the *d/q* components of the converter current consistent with the reference current, with *d-axis* and *q-axis* PI parameters marked as K_{P}^d, K_{I}^d, K_{P}^q, and K_{I}^q. The PLL is utilized to catch the phase information of the PCC, with PI parameters marked as $K_{\mathrm{P}}^{\mathrm{PLL}}$ and $K_{\mathrm{I}}^{\mathrm{PLL}}$.

Let *d-q* reference frame is counterclockwise rotating with the angular frequency of ω, and the phase of *d*-axis leading u_s with θ degrees, which is provided by the phase lock loop (PLL) as shown in Fig. 2(b), the equations that describe the dynamic of

PLL can be written as follows

$$\left.\begin{aligned}\frac{d\theta}{dt} &= \omega - \omega_s \\ \frac{d\omega}{dt} &= K_{\mathrm{P}}^{\mathrm{PLL}}\frac{du_p^q}{dt} + K_{\mathrm{I}}^{\mathrm{PLL}}u_p^q\end{aligned}\right\} \tag{1}$$

where $K_{\mathrm{P}}^{\mathrm{PLL}}$ and $K_{\mathrm{I}}^{\mathrm{PLL}}$ are the proportional and integral parameters.

The voltage balance equations are established in the *d-q* frame as

$$\left.\begin{aligned}u_c^d - u_p^d &= L_c\frac{di_{pr}^d}{dt} + R_c i_{pr}^d - \omega L_c i_{pr}^q \\ u_c^q - u_p^q &= L_c\frac{di_{pr}^q}{dt} + R_c i_{pr}^q + \omega L_c i_{pr}^d\end{aligned}\right\} \tag{2}$$

$$\left.\begin{aligned}u_p^d - u_s^d &= L_l\frac{di_{pr}^d}{dt} + R_l i_{pr}^d - \omega L_l i_{pr}^q \\ u_p^q - u_s^q &= L_l\frac{di_{pr}^q}{dt} + R_l i_{pr}^q + \omega L_l i_{pr}^d\end{aligned}\right\} \tag{3}$$

where $u_s^d$and u_s^q can be written as

$$u_s^d = U_s\cos\theta, \quad u_s^q = -U_s\sin\theta$$

where U_s is the value of the line-to-line voltage of $\boldsymbol{u}_s$.

As shown in Fig. 2(a), the functions of the inner current control loop can be written as follows, (4) shown at the bottom of this page.

B. Steady-State Relationships of Variables

The subscript "0" represents the steady-state value or the equilibrium. The steady-state relationship of voltage and current variables in the *d-q rotational frame* can be expressed as follows

$$\left.\begin{aligned}&i_{pr(0)}^{dref} = i_{pr(0)}^d, \quad i_{pr(0)}^{qref} = i_{pr(0)}^q \\ &x_{d(0)} = R_c i_{pr(0)}^d, \quad x_{q(0)} = R_c i_{pr(0)}^q \\ &\omega_{(0)} = \omega_s, \quad u_{p(0)}^q = 0\end{aligned}\right\} \tag{5}$$

$$\left.\begin{aligned}u_{s(0)}^d &= U_s\cos\theta_{(0)} = u_{p(0)}^d - R_l i_{pr(0)}^d + \omega_s L_l i_{pr(0)}^q \\ -u_{s(0)}^q &= U_s\sin\theta_{(0)} = \omega_s L_l i_{pr(0)}^d + R_l i_{pr(0)}^q\end{aligned}\right\} \tag{6}$$

The steady-state active power and the reactive power exchanged at PCC marked as $P_{c(0)}$ and $Q_{c(0)}$ can be written as follows

$$\left.\begin{aligned}P_{c(0)} &= u_{p(0)}^d i_{pr(0)}^d + u_{p(0)}^q i_{pr(0)}^q = u_{p(0)}^d i_{pr(0)}^d \\ Q_{c(0)} &= u_{p(0)}^q i_{pr(0)}^d - u_{p(0)}^d i_{pr(0)}^q = -u_{p(0)}^d i_{pr(0)}^q\end{aligned}\right\} \tag{7}$$

III. Small Signal Model Based on Electrical Torque Method

Modal analysis results in [22] show that the instability of the grid-connected VSC results from the damping insufficiency of the PLL oscillation mode. To investigate the mechanism insight of the damping insufficiency, the electrical torque approach is employed to establish the small signal model of the studied system in this paper, with which the analytical expressions of the equivalent synchronous and damping coefficients of the studied system can be obtained.

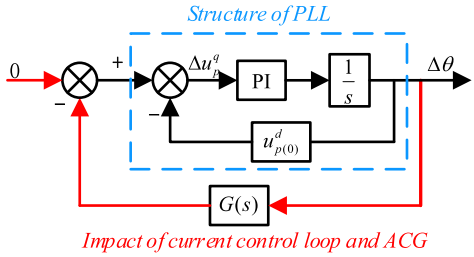

Fig. 3. Developed model reflecting impacts of the current control loop and ACG.

A. PLL Natural Oscillation Mode

To derive the synchronous and damping coefficients of the studied system through the electrical torque approach, PLL is transformed to be a two-order structure similar to the rotor motion of the synchronous generator first.

From (1), the linearized model of PLL can be written as

$$\left.\begin{aligned}\frac{d\Delta\theta}{dt} &= \Delta\omega \\ \frac{d\Delta\omega}{dt} &= (sK_{\mathrm{P}}^{\mathrm{PLL}} + K_{\mathrm{I}}^{\mathrm{PLL}})\Delta u_p^q\end{aligned}\right\} \tag{8}$$

The dynamic of the inner current controller and ACG affect the dynamic of u_p^q, and thus influence the PLL behavior.

To investigate the inherent dynamic of the PLL, the VSC is assumed to be integrated into the infinite bus directly, and thus the dynamic of ACG is overlooked. The following equations hold

$$u_p^d = u_s^d, \quad u_p^q = u_s^q \tag{9}$$

Accordingly

$$\Delta u_p^q = \Delta u_s^q = -U_s\cos\theta_{(0)}\Delta\theta = -u_{s(0)}^d\Delta\theta = -u_{p(0)}^d\Delta\theta \tag{10}$$

It is seen from (10) that the dynamic of u_p^q is only related to the response of PLL and is not affected by the inner current controller. Combining (10) and (8), the PLL inherent dynamic model can be expressed as

$$\left.\begin{aligned}\frac{d\Delta\theta}{dt} &= \Delta\omega \\ \frac{d\Delta\omega}{dt} &= -N_{\mathrm{S}}\Delta\theta - N_{\mathrm{D}}\Delta\omega\end{aligned}\right\} \tag{11}$$

where

$$N_{\mathrm{S}} = u_{p(0)}^d K_{\mathrm{I}}^{\mathrm{PLL}}, \quad N_{\mathrm{D}} = u_{p(0)}^d K_{\mathrm{P}}^{\mathrm{PLL}} \tag{12}$$

N_s and N_D are the natural synchronous and damping coefficients, respectively. The box with blue dot lines in Fig. 3 shows

$$\left.\begin{aligned}u_c^d &= u_p^d + K_{\mathrm{P}}^d(i_{pr}^{dref} - i_{pr}^d) + \int K_{\mathrm{I}}^d(i_{pr}^{dref} - i_{pr}^d)dt - \omega_s L_c i_{pr}^q \\ u_c^q &= u_p^q + K_{\mathrm{P}}^q(i_{pr}^{qref} - i_{pr}^q) + \int K_{\mathrm{I}}^q(i_{pr}^{qref} - i_{pr}^q)dt + \omega_s L_c i_{pr}^d\end{aligned}\right\} \tag{4}$$

the transfer function of the system with only PLL dynamics involved.

Based on (11), the frequency ω_n and damping ζ_n of PLL natural oscillation mode can be obtained as

$$\omega_n \approx \sqrt{u^d_{p(0)} K^{\mathrm{PLL}}_{\mathrm{I}}} \quad \zeta_n = \frac{u^d_{p(0)} K^{\mathrm{PLL}}_{\mathrm{P}}}{2\sqrt{u^d_{p(0)} K^{\mathrm{PLL}}_{\mathrm{I}}}} \tag{13}$$

It is seen from (11) and (12) that the natural oscillation frequency is related only to the voltage at PCC and the integral parameter of PLL. Moreover, both the natural synchronous and damping coefficients are positive, indicating that the natural dynamic of the PLL behaves as a damped oscillation. It can be concluded that the PLL controller is stable when the inner current controller and ACG are overlooked.

B. Impacts of the Current Control Loop and ACG on PLL

Following, the impacts of the current control loop and ACG is derived to be attached to the two-order PLL structure.

Substituting (2) into (4), and eliminating the variables of u^d_c ,u^q_c, u^d_p and u^q_p , yields

$$\left.\begin{array}{l} K^d_{\mathrm{P}}(i^{dref}_{pr} - i^d_{pr}) + \int K^d_{\mathrm{I}}(i^{dref}_{pr} - i^d_{pr})dt - R_c i^d_{pr} \\ = L_c \frac{di^d_{pr}}{dt} - (\omega - \omega_s) L_c i^q_{pr} = L_c \frac{di^d_{pr}}{dt} - L_c i^q_{pr} \frac{d\theta}{dt} \\ K^q_{\mathrm{P}}(i^{qref}_{pr} - i^q_{pr}) + \int K^q_{\mathrm{I}}(i^{qref}_{pr} - i^q_{pr})dt - R_c i^q_{pr} \\ = L_c \frac{di^q_{pr}}{dt} + (\omega - \omega_s) L_c i^d_{pr} = L_c \frac{di^q_{pr}}{dt} + L_c i^d_{pr} \frac{d\theta}{dt} \end{array}\right\} \tag{14}$$

Combining (3) and (14), and eliminating the differential items, the following equation can be held

$$\begin{aligned} \begin{bmatrix} u^d_p \\ u^q_p \end{bmatrix} - \begin{bmatrix} u^d_s \\ u^q_s \end{bmatrix} &= \frac{L_l}{L_c} \begin{bmatrix} K^d_{\mathrm{P}}(i^{dref}_{pr} - i^d_{pr}) \\ K^q_{\mathrm{P}}(i^{qref}_{pr} - i^q_{pr}) \end{bmatrix} \\ &+ \frac{L_l}{L_c} \begin{bmatrix} \int K^d_{\mathrm{I}}(i^{dref}_{pr} - i^d_{pr})dt \\ \int K^q_{\mathrm{I}}(i^{qref}_{pr} - i^q_{pr})dt \end{bmatrix} \\ &- \frac{L_l R_c}{L_c} \begin{bmatrix} i^d_{pr} \\ i^q_{pr} \end{bmatrix} + \begin{bmatrix} R_l & -\omega_s L_l \\ \omega_s L_l & R_l \end{bmatrix} \begin{bmatrix} i^d_{pr} \\ i^q_{pr} \end{bmatrix} \end{aligned} \tag{15}$$

Linearizing (14) and (15) around its equilibrium and taking the *Laplace* transform of linearized equations, we obtain the frequency domain equations

$$\left.\begin{array}{l} B_d(s)\Delta i^d_{pr} = L_c i^q_{pr(0)} s\Delta\theta \\ B_q(s)\Delta i^q_{pr} = -L_c i^d_{pr(0)} s\Delta\theta \end{array}\right\} \tag{16}$$

$$\left.\begin{array}{l} \Delta u^d_p = \Delta u^d_s + \left[R_l - \frac{L_l}{L_c} C_d(s)\right] \Delta i^d_{pr} - \omega_s L_l \Delta i^q_{pr} \\ \Delta u^q_p = \Delta u^q_s + \left[R_l - \frac{L_l}{L_c} C_q(s)\right] \Delta i^q_{pr} + \omega_s L_l \Delta i^d_{pr} \end{array}\right\} \tag{17}$$

where

$$\begin{array}{l} C_d(s) = K^d_{\mathrm{P}} + K^d_{\mathrm{I}}/s + R_c, \quad C_q(s) = K^q_{\mathrm{P}} + K^q_{\mathrm{I}}/s + R_c \\ B_d(s) = C_d(s) + sL_c, \quad B_q(s) = C_q(s) + sL_c \end{array}$$

Combing (6), (16) and (17), the following equation can be held

$$\begin{aligned} &\Delta u^q_p \\ &= \left[-u^d_{p(0)} - \frac{C_d(s)}{B_d(s)} \omega L_l i^q_{pr(0)} + \frac{C_q(s)}{B_q(s)} (R_l + sL_l) i^d_{pr(0)}\right] \Delta\theta \end{aligned} \tag{18}$$

To simplify the analysis, the *d*- and *q-axis* PI parameters of the inner current controller are set as proportional to the equivalent resistance and inductance of the converter phasor reactor in this study. That is

$$\frac{R_c}{K^d_{\mathrm{I}}} = \frac{L_c}{K^d_{\mathrm{P}}} = \frac{R_c}{K^q_{\mathrm{I}}} = \frac{L_c}{K^q_{\mathrm{P}}} = \sigma \tag{19}$$

where σ is the time constant of the inner current controller.

Combing (18) and (19), it has

$$\frac{C_d(s)}{B_d(s)} = \frac{1}{1 + s\sigma} + \frac{R_c}{K^d_{\mathrm{P}} + K^d_{\mathrm{I}}/s + sL_c + R_c} \tag{20}$$

As σ is generally set as several milliseconds to make sure the fast inner-current regulation of VSC, R_c is negligible compared to K^d_{P} and K^d_{I}. Consequently, the following equations can be obtained

$$\frac{C_d(s)}{B_d(s)} = \frac{C_q(s)}{B_q(s)} = \frac{1}{1 + \sigma s} \tag{21}$$

In addition, the line resistance is usually relatively smaller than the line reactance and can be ignored during stability analysis, that is

$$R_l = 0 \tag{22}$$

Submitting (21) and (22) to (18), the small-signal of u^q_p can be written as

$$\Delta u^q_p = -u^d_{p(0)} \Delta\theta - G(s)\Delta\theta \tag{23}$$

where

$$G(s) = \frac{1}{1 + \sigma s} (\omega_s L_l i^q_{pr(0)} - sL_l i^d_{pr(0)}) \tag{24}$$

The transfer function $G(s)$ represents the impacts of the dynamics of the current control loop and ACG on PLL, as shown in Fig. 3.

C. Two-Order Model of the Grid-Connected VSC

Combining (8) and (23), the small signal model of the grid-connected VSC considering the impacts of the current control loop and ACG can be written as follows

$$\begin{aligned} &\frac{d}{dt} \begin{bmatrix} \Delta\theta \\ \Delta\omega \end{bmatrix} \\ &= \begin{bmatrix} 0 & 1 \\ -N_{\mathrm{S}} - K^{\mathrm{PLL}}_{\mathrm{I}} G(s) & -N_{rmD} - K^{\mathrm{PLL}}_{\mathrm{P}} G(s) \end{bmatrix} \begin{bmatrix} \Delta\theta \\ \Delta\omega \end{bmatrix} \end{aligned} \tag{25}$$

The above model can be written in a two-order differential equation as follows

$$\frac{d^2\Delta\theta}{dt^2} = -\left[N_{\mathrm{S}} + K^{\mathrm{PLL}}_{\mathrm{I}} G(s)\right] \Delta\theta - \left[N_{\mathrm{D}} + K^{\mathrm{PLL}}_{\mathrm{P}} G(s)\right] \Delta\omega \tag{26}$$

Based on the electrical torque method [19], system damping torque is proportional to the state variable $\Delta\omega$, while system synchronous torque is proportional to the state variable $\Delta\theta$. Considering the relationship of $s\Delta\theta = \Delta\omega$, and substituting $s = j\omega_n$ into (26), it has

$$\frac{d^2\Delta\theta}{dt^2} = -K_{\mathrm{S}}\Delta\theta - K_{\mathrm{D}}\Delta\omega \tag{27}$$

where

$$K_{\mathrm{S}} = K_{\mathrm{I}}^{\mathrm{PLL}}(u_{p(0)}^{d} + \mathrm{Re}[G(j\omega_n)]) - K_{\mathrm{P}}^{\mathrm{PLL}}\omega_n \mathrm{Im}[G(j\omega_n)] \tag{28}$$

$$K_{\mathrm{D}} = K_{\mathrm{P}}^{\mathrm{PLL}}(u_{p(0)}^{d} + \mathrm{Re}[G(j\omega_n)]) + K_{\mathrm{I}}^{\mathrm{PLL}}\frac{\mathrm{Im}\left[G(j\omega_n)\right]}{\omega_n} \tag{29}$$

K_{S} and K_{D} are the equivalent synchronous and damping coefficients.

Based on the electrical torque approach, the studied system has been modeled as a two-order model, as shown in (27), which clearly describes the system dynamic characteristic. The system stability can be judged by the sign of the equivalent synchronous and damping coefficients. If $K_{\mathrm{S}} < 0$, monotonic divergence happens. And if $K_{\mathrm{S}} > 0$ while$K_{\mathrm{D}} < 0$, increasing amplitude oscillation will occur.

IV. Stability Analysis Using the Proposed Model

The equivalent two-order model of the VSC grid-connected system as (27) has been derived in the previous section. Following the oscillation characteristics of dominated unstable mode, including the frequency and damping characteristics, affected by operation conditions and system parameters are investigated.

Based on (6) and ignoring R_l, $u_{p(0)}^{d}$ can be represented by a combination of $i_{pr(0)}^{d}$ and $i_{pr(0)}^{q}$ as

$$u_{p(0)}^{d} = -\omega_s L_l i_{pr(0)}^{q} + \sqrt{U_s^2 - \left(\omega_s L_l i_{pr(0)}^{d}\right)^2}. \tag{30}$$

Substituting (24) and (30) to (28) and (29), the analytical expressions of synchronous and damping coefficients can be calculated as

$$\begin{aligned} K_{\mathrm{S}} = {} & K_{\mathrm{I}}^{\mathrm{PLL}}[\sqrt{U_s^2 - \left(\omega_s L_l i_{pr(0)}^{d}\right)^2} - \tfrac{\omega_n^2 \sigma L_l (i_{pr(0)}^{d} + \omega_s \sigma i_{pr(0)}^{q})}{1+(\omega_n\sigma)^2}] \\ & + K_{\mathrm{P}}^{\mathrm{PLL}} \tfrac{\omega_n^2 L_l (i_{pr(0)}^{d} + \omega_s \sigma i_{pr(0)}^{q})}{1+(\omega_n\sigma)^2} \end{aligned} \tag{31}$$

$$\begin{aligned} K_{\mathrm{D}} = {} & K_{\mathrm{P}}^{\mathrm{PLL}}\left[\sqrt{U_s^2 - \left(\omega_s L_l i_{pr(0)}^{d}\right)^2} - \tfrac{\omega_n^2 \sigma L_l (i_{pr(0)}^{d} + \omega_s \sigma i_{pr(0)}^{q})}{1+(\omega_n\sigma)^2}\right]. \\ & - K_{\mathrm{I}}^{\mathrm{PLL}} \tfrac{L_l (i_{pr(0)}^{d} + \omega_s \sigma i_{pr(0)}^{q})}{1+(\omega_n\sigma)^2} \end{aligned} \tag{32}$$

The frequency and damping characteristics can be drawn from the analytical expression of synchronous and damping coefficients as shown in (31) and (32).

A. Frequency Characteristic

Comparing (32) to (31), K_{S} is apparently positive, and K_{D} is far smaller than K_{S}. Consequently, step-respond of the studied system is in the form of oscillation, and the oscillation frequency is determined by K_{S}, which can be approximated as

$$\omega_d \approx \sqrt{K_{\mathrm{S}}}. \tag{33}$$

Comprehensively considering the responding frequency and filtering characteristics, it usually has $K_{\mathrm{P}}^{\mathrm{PLL}} \ll K_{\mathrm{I}}^{\mathrm{PLL}}$ [23], then K_{S} can be simplified as

$$\begin{aligned} K_{\mathrm{S1}} = K_{\mathrm{I}}^{\mathrm{PLL}} \Bigg[& \sqrt{U_s^2 - \left(\omega_s L_l i_{pr(0)}^{d}\right)^2} \\ & - \omega_n^2 \sigma L_l (i_{pr(0)}^{d} + \omega_s \sigma i_{pr(0)}^{q}) \Bigg]. \end{aligned} \tag{34}$$

It is seen from (34) that the synchronous coefficient is mainly determined by the integral coefficient of PLL and the system voltage. The larger $K_{\mathrm{I}}^{\mathrm{PLL}}$ or U_s is, the higher the synchronous coefficient is. Thus, the system oscillates with a higher frequency.

(30) shows that the increase of L_l, $i_{pr(0)}^{d}$ and $i_{pr(0)}^{q}$ will lead to voltage drop at PCC, which results in a decrease in oscillation frequency.

In addition, (31) also indicates that increasing $K_{\mathrm{P}}^{\mathrm{PLL}}$ will increase the synchronous torque, thus increase the oscillation frequency.

B. Damping Characteristic

Based on (27), the damping ratio of the studied system can be calculated as

$$\zeta = \frac{K_{\mathrm{D}}}{2\sqrt{K_{\mathrm{S}}}} \tag{35}$$

The system is small signal stable under the condition that its damping coefficient is positive. Comparing (32) to (12), it is evident that dynamics of the current control loop and ACG introduce a negative growth in system damping coefficient, which will result in insufficient damping of the PLL oscillation mode, thus leading to the small-signal instability of the studied system.

It is seen from (32) that K_{D} is directly expressed by the operation and the system parameters, i.e., U_s, $i_{pr(0)}^{d}$, $i_{pr(0)}^{q}$, $K_{\mathrm{P}}^{\mathrm{PLL}}$, $K_{\mathrm{I}}^{\mathrm{PLL}}$ and L_l. The impacts of the operation and system parameters on the system stability are as follows.

Firstly, a stable system voltage is critical for the stable operation of a power system. A drop in $U_s$will lead to an increase in $i_{pr(0)}^{d}$. As is seen from (32), both the decreasing $U_s$and the increasing $i_{pr(0)}^{d}$ induce a decrease in K_{D}, and thus worsen the system stability.

For a fixed infinite voltage U_s, it is seen from (32) that the system damping coefficient decrease with increasing $i_{pr(0)}^{d}$, $i_{pr(0)}^{q}$ or L_l, thus the system stability is worsened. That is, increasing the active power generation, absorbing reactive power, or increasing the electrical distance will worsen the system stability.

Defining the time constant of PLL as

$$\sigma_{\mathrm{PLL}} = \frac{K_{\mathrm{P}}^{\mathrm{PLL}}}{K_{\mathrm{I}}^{\mathrm{PLL}}}. \tag{36}$$

For a fixed $K_{\mathrm{I}}^{\mathrm{PLL}}$, K_{D} increase with σ_{PLL}. As a result, the system stability is enhanced.

On the other hand, for a fixed σ_{PLL}, ω_n in (32) increases with $K_{\mathrm{I}}^{\mathrm{PLL}}$, which implies the positive part of K_{D} increases more significant than the negative part. As a result, K_{D} is more likely to stay above zero. It can be concluded that when σ_{PLL} is fixed, the higher $K_{\mathrm{I}}^{\mathrm{PLL}}$ is, the more stable the system is.

C. Analytical Stability Criterion

Considering $K_{\mathrm{P}}^{\mathrm{PLL}} \ll K_{\mathrm{I}}^{\mathrm{PLL}}$ and $\omega_n\sigma \ll 1$, (32) can be simplified as

$$K_{\mathrm{D2}} = K_{\mathrm{P}}^{\mathrm{PLL}}\sqrt{U_s^2 - \left(\omega_s L_l i_{pr(0)}^d\right)^2} - K_{\mathrm{I}}^{\mathrm{PLL}} L_l (i_{pr(0)}^d + \omega_s\sigma i_{pr(0)}^q). \tag{37}$$

A two-order dynamic system is small-signal stable when the damping torque is positive. That is

$$K_{\mathrm{D}} > 0. \tag{38}$$

Combing (36), (37) and (38), the stability condition of the grid-connected VSC can be expressed as follows

$$\sigma_{\mathrm{PLL}} > \frac{L_l(i_{pr(0)}^d + \omega_s\sigma i_{pr(0)}^q)}{\sqrt{U_s^2 - \left(\omega_s L_l i_{pr(0)}^d\right)^2}} = \sigma_0. \tag{39}$$

(39) provides an analytical stability criterion for the grid-connected VSC. The system stability can be judged directly through the system parameters and the operation conditions through (39), without complex eigenvalue calculation or Bode diagram analysis. Furthermore, it can be clearly drawn from (39) that a low infinite source voltage, heavy load, reactive power absorption, and high SCR will deteriorate system stability.

Usually, to make full use of the rated capacity of the converter, the unit power factor control mode is utilized in grid-connected VSC. That is

$$Q_{c(0)} = 0,\ i_{pr(0)}^q = 0. \tag{40}$$

Combing (39) with (40), the analytical stability condition under unite power factor control can be written as

$$\sigma_{\mathrm{PLL}} > \frac{L_l i_{pr(0)}^d}{\sqrt{U_s^2 - \left(\omega_s L_l i_{pr(0)}^d\right)^2}}. \tag{41}$$

Combing (41) with (6), (7) and (40), the maximum transmission power which ensures system stability can be calculated as

$$P_{c(0)}^{\max} = \frac{(\sigma_{\mathrm{PLL}} R_l + L_l)\sigma_{\mathrm{PLL}} U_s^2}{(1 + \omega_s^2\sigma_{\mathrm{PLL}}^2)L_l^2}. \tag{42}$$

(42) bridges an analytical relationship among the transmission power limitation, the electrical distance and the controller parameters.

TABLE I
PARAMETERS OF GRID-CONNECTED VSC

Symbol	Item	Value
U_s	Line voltage of the infinite bus	220 kV
S_B	The base capacity of the studied system	200 MVA
L_l	The inductance of transmission line	0.5 p.u.
R_l	The resistance of transmission line	0.05 p.u.
L_c	The inductance of the phase reactor	0.15 p.u.
R_c	The resistance of the phase reactor	0.001 p.u.
ω_s	Fixed system angular frequency	314 rad/s
$K_{\mathrm{P}}^d = K_{\mathrm{P}}^q$	Proportional gain of fast current control	38.51
$K_{\mathrm{I}}^d = K_{\mathrm{I}}^q$	Integral gain of fast current control	80.67
σ	The time constant of inner current control	3 ms
$K_{\mathrm{P}}^{\mathrm{PLL}}$	Proportional gain of PLL	0.2
$K_{\mathrm{I}}^{\mathrm{PLL}}$	Integral gain of PLL	100
σ_{PLL}	The time constant of PLL	2 ms

TABLE II
COMPARISON OF DIFFERENT ANALYTICAL MODELS OF GRID-CONNECTED VSC

Operation conditions	Full-order model	Proposed model
P = 180MW Q = 0MVar	-3.39±123.73j	-2.32±123.56j
P = 200MW Q = 10MVar	-2.23±121.53j	-0.99±121.15j
P = 200MW Q = 0MVar	-0.51±119.97j	0.80±119.67j
P = 200MW Q = −10MVar	1.81±117.47j	3.25±117.33j
P = 220MW Q = 0MVar	4.97±110.78j	6.76±110.25j

V. SIMULATIONS VERIFICATION

The case of a single VSC connected to an infinite bus through the transmission line is utilized to investigate the small signal stability of the grid-connected VSC. The detailed parameters of the case study can be referred in Table I. The following two aspects are verified through eigenvalue analysis and electromagnetic transient simulation:

1) the reliability and sufficiency of the proposed two-order model and the analytical stability criterion;
2) the impacts of operation conditions and system parameters on system stability.

A. Reliability and Conservatism of the Proposed Model

Both the full six-order model described by (2)–(4) and the proposed two-order model described by (27) are established in MATLAB. The eigenvalues of the two models under different conditions are shown in Table II. And the calculation results of (39) and (42) are shown in Table III and Fig. 4.

Table II exhibitions the dominated poles calculated from the above two models of the grid-connected VSC under different active and reactive power references. As shown in Table II, the real parts of the eigenvalues calculated from the proposed two-order model are always slightly larger than those of the full-order model, while the imaginary parts are nearly the same. The ignorance of the system resistances moves the dominated eigenvalues of the system to the right of the complex plane.

TABLE III
COMPARISON BETWEEN (39) AND THE FULL-ORDER MODEL

Operation conditions		$P_c = 203$MW $Q_c = 0$Mvar	$P_c = 200$MW $Q_c = -3$Mvar	$P_c = 180$MW $Q_c = -20$Mvar
σ_0 (ms)		2.28	2.29	2.27
σ_{PLL} (ms)	1.8	1.33±118.9i	1.41±119.1i	1.45±120.6i
	2.0	0.018±119.2i	0.095±119.4i	1.08±120.9i
	2.2	-1.30±119.5i	-1.23±119.7i	-1.25±121.24i
	2.4	-2.64±119.8i	-2.56±119.9i	-2.62±121.54i

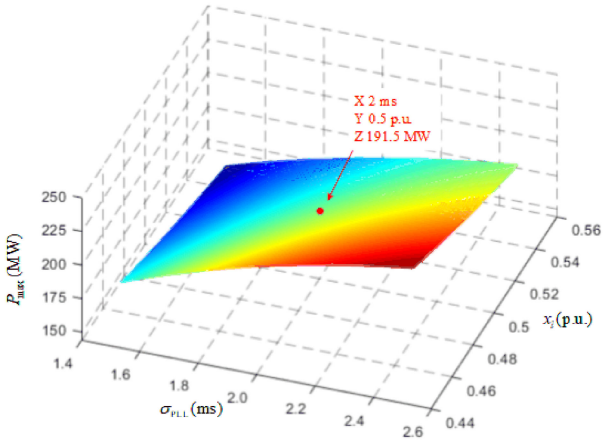

Fig. 4. Stable region of renewable generation for VSC.

Thus, the reliability and sufficiency of the proposed two-order model can be guaranteed.

The critical stable $\sigma_0$calculated from (39) under different operation conditions are shown in the 2nd row of Table III, and the 3rd to 6th rows are the eigenvalues of the full-order model under different σ_{PLL}. It is seen from Table III that the increasing σ_{PLL}will enhance the system stability, which is in agreement with (39). In addition, $\sigma_{\text{PLL}} > \sigma_0$can make sure the system stability, while the system may also keep stable when $\sigma_{\text{PLL}} < \sigma_0$ under critical stable conditions. The calculated critical σ_0 can make sure the system stability. The sufficiency of (39) has been verified.

The maximum renewable generation of VSC varying with the time constant of PLL σ_{PLL} and the transmission line reactance x_l is shown in Fig. 4. It is seen from Fig. 4 that the maximum renewable generation of VSC increases with σ_{PLL} and decreases x_l. The stable renewable generation limitation under the standard system parameters ($\sigma_{\text{PLL}} = 2$, $x_l = 0.5$ p.u.) calculated from (42) is 191.5 MW. However, Table II shows that the system still keeps stable under the active power generation of 200 MW. The maximum renewable generation calculated from (42) is conservative.

B. Impact of System Parameters on System Stability

As is drawn from the proposed two-order model, the oscillation mode of the grid-connected VSC is closely related to U_s, $i^d_{pr(0)}$, $i^q_{pr(0)}$, $K_{\text{P}}^{\text{PLL}}$, $K_{\text{I}}^{\text{PLL}}$ and L_l. The damping ratio and oscillation frequency calculated from the full six-order model and

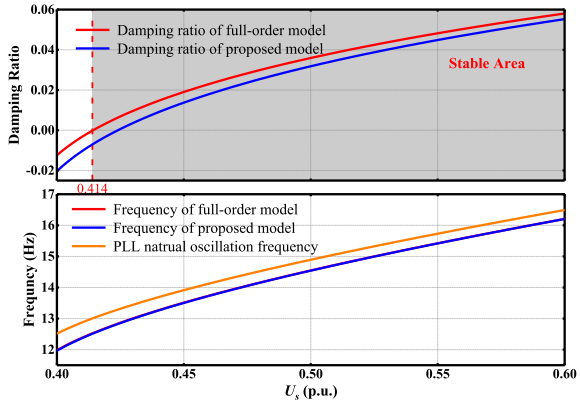

Fig. 5. Damping and frequency varying with the infinite source voltage.

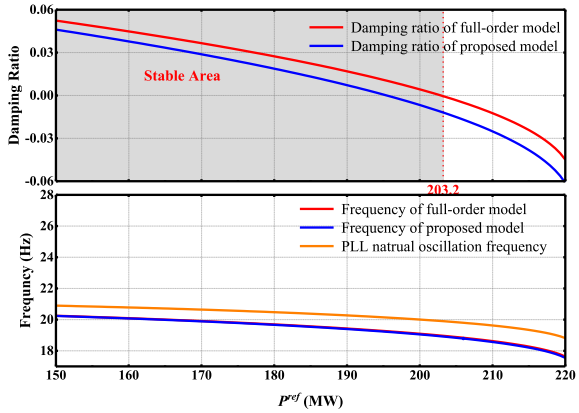

Fig. 6. Damping and frequency varying with the active power reference.

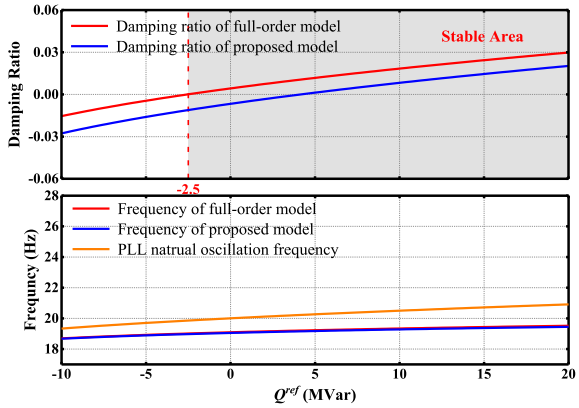

Fig. 7. Damping and frequency varying with the reactive power reference.

the proposed two-order model varying with system parameters are shown in Figs. 5–10. It can be seen from Figs. 5–10 that the damping ratio and frequency calculated from the proposed two-order model are close to those calculated from the full six-order model. Furthermore, the former is always less damped than the latter. It can be concluded that the stability analysis results from the proposed two-order model are reliable and conservative.

The impacts of critical factors on the system oscillation mechanism are described in detail.

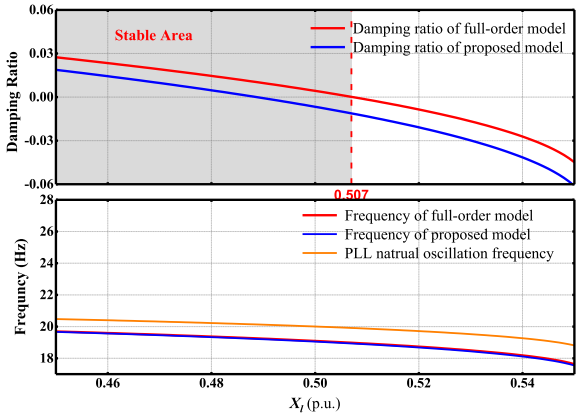

Fig. 8. Damping and frequency varying with the line inductance.

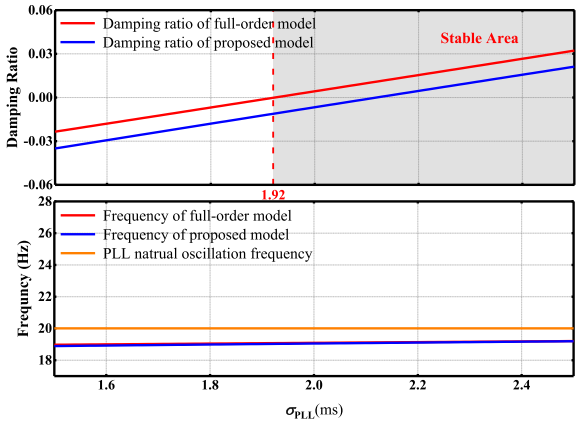

Fig. 9. Damping and frequency varying with the time constant of PLL.

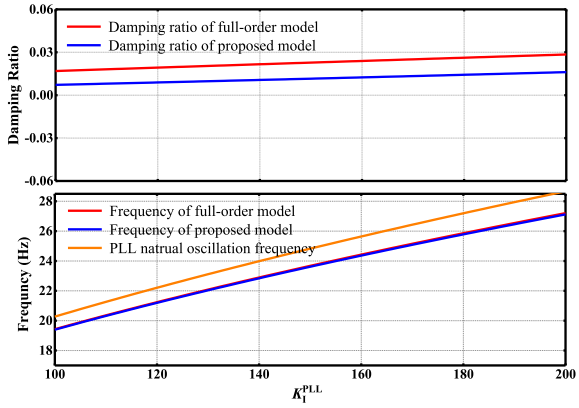

Fig. 10. Damping and frequency varying with the integral parameter of PLL.

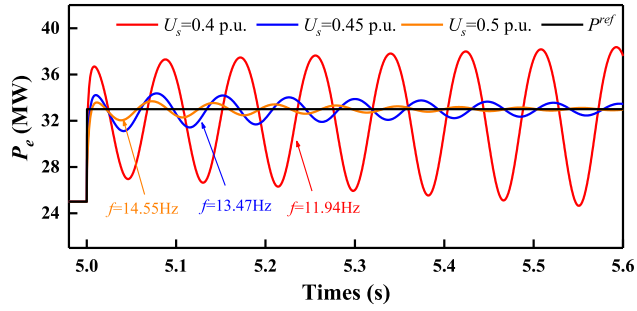

Fig. 11. Small signal response with different infinite source voltages.

1) *Impact of infinite source voltage*: Usually, the wind turbines are required to have the ability of low voltage ride through (LVRT). It is necessary to investigate the small-signal stability of the grid-connected VSC under low voltage levels. Setting the active power reference as 33 MW and varying the infinite source voltage from 0.4 pu to 0.6 pu, the damping ratio and frequency characteristics are shown in Fig. 5. It is seen from Fig. 5 that both the damping and frequency of the oscillation mode decrease apparently along with the decreasing infinite source voltage, indicating that a lower infinite source voltage will worsen the system stability, and the oscillation frequency is also reduced. The transmitted active power should be minimized to keep the system stable during LVRT.
2) *Impact of active power reference*: In order to investigate the impact of the active power generation on system stability, system parameters are fixed, and the reactive power reference is set as 0 MVar. Varying the active power reference from

150 MW to 220 MW, the damping ratio and frequency characteristics are shown in Fig. 6. It is seen from Fig. 6 that the damping ratio of the dominated poles increases along with the active power and shifts from positive to negative, while its calculated frequency decreases slightly. It indicates that an increasing active power reference will worsen the system stability and slightly reduce the oscillation frequency, which is entirely consistent with the theoretical analysis.

3) *Impact of reactive power reference*: The impact of the reactive power reference of VSC on system stability is shown in Fig. 7, where system parameters are fixed, and the active power reference is set as 200 MW. As shown in Fig. 7, both the damping ratio and frequency of the oscillation mode increase with reactive power reference. From the view of the electrical torque method, emitting reactive power from the converter results in a negative *q-axis* current, increasing the damping coefficient and enhancing the system stability, while the absorption of reactive power acts oppositely.
4) *Impact of line inductance*: As a reflection of AC grid strength, the transmission line inductance also influences the stability of the studied system. Varying the line inductance, the damping ratio and frequency characteristics are shown in Fig. 8, with the active power reference set as 200 MW and the reactive power set as 0 MVar. As shown in Fig. 8, the damping ratio of the oscillation mode decreases with increasing line reactance, while its frequency decreases slightly. It indicates that an increasing electrical distance is detrimental to the small-signal stability. Based on the electrical torque approach, increasing line inductance can reduce both the system synchronous and damping coefficients, which means the frequency and damping of the oscillation mode are both decreased. The electrical torque approach-based analysis is consistent with eigenvalue calculation.
5) *Impact of PLL parameters*: Based on the above analysis, it is known that both the synchronous and damping coefficients are closely related to PLL parameters. The

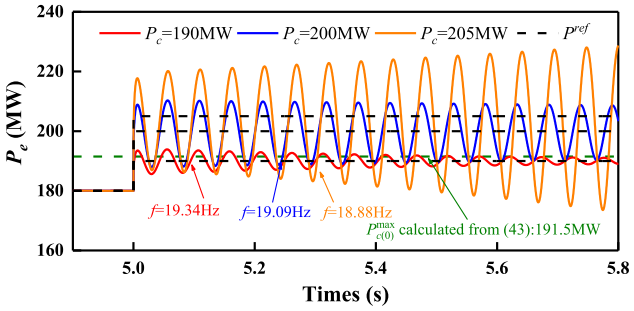

Fig. 12. Small signal response with different active power references.

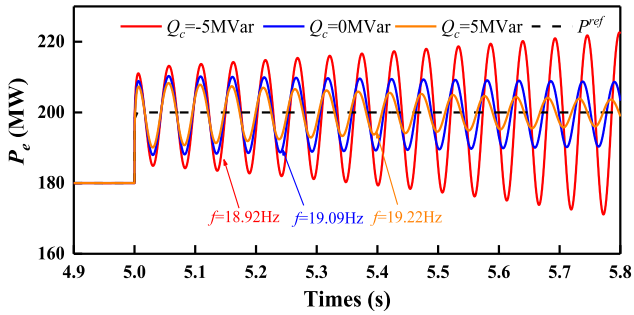

Fig. 13. Small signal response with different reactive power references.

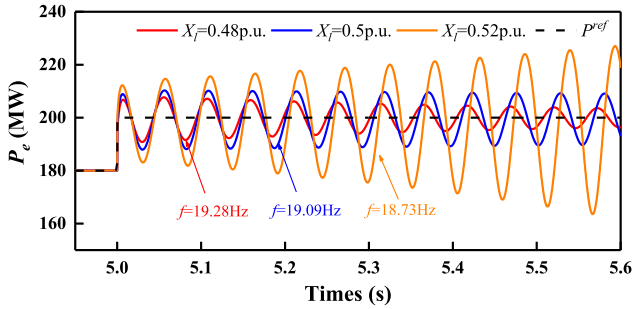

Fig. 14. Small signal response with different line inductances.

impacts of PLL parameters on the unstable oscillation mode are shown in Figs. 9 and 10. As demonstrated from Fig. 9, both the frequency and damping ratio of the dominated oscillation mode increase with the time inertia constant of PLL under fixed integral parameter, which can also be explained by the proposed two-order model. On the one hand, the synchronous coefficient increases with $K_{\mathrm{P}}^{\mathrm{PLL}}$, which is reflected by an increase in the oscillation frequency. On the other hand, the stability margin of VSC increases with larger σ_{PLL} from (39).

As shown in Fig. 10, when the time constant of PLL is fixed at 2ms, the system oscillation frequency increases with the integral parameter of PLL, while the damping ratio is increased slightly. It well verified that the oscillation frequency of the grid-connected VSC is mainly influenced by the integral parameter of PLL. In addition, increasing $K_{\mathrm{I}}^{\mathrm{PLL}}$ under fixed σ_{PLL} is also beneficial for system stability but is not significantly.

The eigenvalue calculation results exhibit the frequency and damping characteristics of the dominated mode affected by operation points and system parameters, which are entirely consistent with the results drawn from the proposed two-order model. In addition, the frequencies calculated from the two models are nearly the same. Consequently, using the electrical torque model can directly evaluate the stability of the grid-connected VSC and estimate its oscillation frequency, which is conducive to studying the resonance between the VSC and other components.

C. Nonlinear Simulation

In order to verify the theoretical results of the small signal stability of the grid-connected VSC, the detailed electromagnet transient simulation model of the grid-connected VSC is built with the PSCAD/EMTDC software, and a mutation of the active power generation is used to simulate the small disturbance of the studied system.

The nonlinear simulation results under different infinite source voltages are shown in Fig. 11. The active power reference is mutated from 25 MW to 33 MW at 5 s, and the infinite source voltage is set as 0.4 pu, 0.45 pu, and 0.5 pu, respectively. It is seen from Fig. 11 that the active power curve oscillates with an increasing amplitude under a lower voltage level, and the frequency is decreased. A low infinite source voltage will reduce the system stability and the oscillation frequency.

Fig. 12 shows the simulation results under different disturbances, where the active power reference is mutated from 180 MW to 190 MW, 200 MW, and 205 MW at 5 s, respectively. It is seen that the active power curve from the converter divergent gradually, and the frequency decreases slightly with increasing active power reference. The result agrees with the theoretical analysis in Section III that a higher active power reference will worsen the system stability and reduce the oscillation frequency. In addition, Fig. 12 shows that the system is in a critical stable state under the active power reference of 200 MW. Based on the proposed two-order model, the critical active power generation for VSC under the unit power factor control mode is 191.5 MW. The nonlinear simulation results further testify to the conservatism of the proposed two-order model.

Simulated responses that verify the small signal stability affected by the reactive power reference are shown in Fig. 13. The active power reference is mutated from 180 MW to 200 MW at 5 s, and the reactive power references are set as −5MVar, 0 MVar, and 5 MVar, respectively. Fig. 13 indicates that the increasing reactive power reference results in a damped oscillation with a higher frequency, which is consistent with the above theoretical analysis.

Fig. 14 shows the simulation results under different line inductances when the active power reference is mutated from 180 MW to 200 MW at 5 s, and the line inductances are set as 0.48 pu, 0.5 pu, and 0.52 pu, respectively. When the line inductance is increased, both the full synchronous and damping coefficients of the VSC grid-connected system decrease. Due to the negative damping contributed by larger line inductance, the apparent oscillation is observed in Fig. 14, while the frequency decreases slightly.

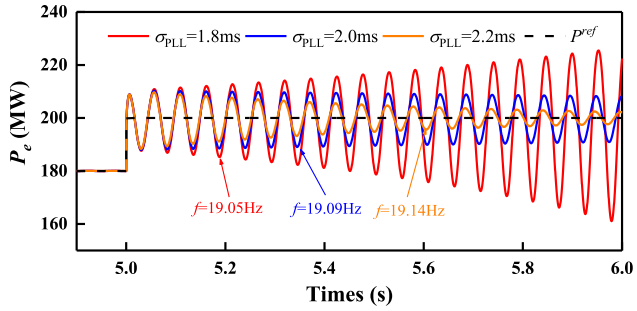

Fig. 15. Small signal response with different time constants of PLL.

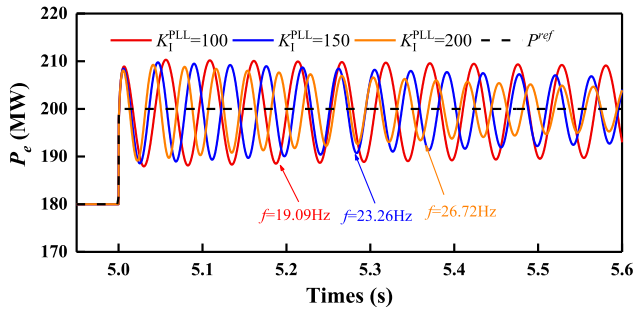

Fig. 16. Small signal response with different integral parameters of PLL.

To further verify small signal stability affected by PLL parameters, nonlinear simulations are shown in Figs. 15 and 16. The active power reference is mutated from 180 MW to 200 MW at 5 s, and the PLL time constant is set as 1.8 ms, 2 ms, and 2.2 ms, respectively. When the time constant of PLL increases, both the synchronous and the damping coefficients increase. Consequently, the oscillation of the active power curve from the converter is suppressed, and its frequency increases, as observed in Fig. 15.

Fixing the time constant of PLL as 2 ms and setting its integral parameter as 100, 150, and 200, respectively, the dynamic responses of the active power with the active power reference mutated from 180 MW to 200 MW at 5 s is shown in Fig. 16. Fig. 16 shows that oscillation with an obviously larger frequency occurs as the integral parameter increases, while it decays faster. The results are fully consistent with the theoretical analysis results.

VI. Conclusion

Small-signal stability for the grid-connected VSC is fully discussed in this paper using the electric torque approach. A two-order model of the studied system is established based on the electrical torque approach, with analytical expressions of the synchronous and damping coefficients. Accordingly, stability analysis and oscillation frequency are drawn from the proposed two-order model. Conclusions are as follows:

- The qualitative evaluation from the damping coefficient indicates that a small PLL time constant, low infinite source voltage, heavy load, reactive power absorption, and long electrical distance will deteriorate system stability.
- An analytical stability criterion is obtained from the damping coefficient, providing a direct quantitative system stability judgment based on the system parameters and operation conditions.
- The oscillation frequency of the studied system is mainly determined by the infinite source voltage and the integral parameter of PLL, and the other condition can also influence it but not obviously. Moreover, the oscillation frequency can be estimated from the synchronous coefficient, which provides theoretical guidance for the resonance induced by the VSC.

References

[1] J. Hu, Y. Huang, D. Wang, H. Yuan, and X. Yuan, "Modeling of grid-connected DFIG-Based wind turbines for DC-link voltage stability analysis," *IEEE Trans. Sustain Energy*, vol. 6, no. 4, pp. 1325–1336, Oct. 2015.

[2] L. Cai and I. Erlich, "Doubly fed induction generator controller design for the stable operation in weak grids," *IEEE Trans. Sustain Energy*, vol. 6, no. 3, pp. 1078–1084, Jul. 2015.

[3] D. Zhang, Y. Wang, J. Hu, S. Ma, Q. He, and Q. Guo, "Impacts of PLL on the DFIG-based WTG's electromechanical response under transient conditions: Analysis and modeling," *CSEE J. Power Energy*, vol. 2, no. 2, pp. 30–39, Jun. 2016.

[4] Y. Li, Z. Xu, J. Østergaard, and D. J. Hill, "Coordinated control strategies for offshore wind farm integration via VSC-HVDC for system frequency support," *IEEE Trans. Energy Convers.*, vol. 32, no. 3, pp. 843–856, Sep. 2017.

[5] W. Wang, Y. Li, Y. Cao, U. Häger, and C. Rehtanz, "Adaptive droop control of VSC-MTDC system for frequency support and power sharing," *IEEE Trans. Power Syst.*, vol. 33, no. 2, pp. 1264–1274, Mar. 2018.

[6] G. Wu, Z. Du, C. Li, and G. Li, "VSC-MTDC operation adjustments for damping inter-area oscillations," *IEEE Trans. Power Syst.*, vol. 34, no. 2, pp. 1373–1382, Mar. 2019.

[7] X. Wang, L. Harnefors, and F. Blaabjerg, "Unified impedance model of grid-connected voltage-source converters," *IEEE Trans. Power Electron.*, vol. 33, no. 2, pp. 1775–1787, Feb. 2018.

[8] Y. Huang, X. Yuan, J. Hu, and P. Zhou, "Modeling of VSC connected to weak grid for stability analysis of DC-Link voltage control," *IEEE J. Emerg. Sel. Top. Power Electron.*, vol. 3, no. 4, pp. 1193–1204, Dec. 2015.

[9] H. Zhang, L. Harnefors, X. Wang, H. Gong, and J. Hasler, "Stability analysis of grid-connected voltage-source converters using SISO modeling," *IEEE Trans. Power Electron.*, vol. 34, no. 8, pp. 8104–8117, Aug. 2019.

[10] J. Z. Zhou, H. Ding, S. Fan, Y. Zhang, and A. M. Gole, "Impact of short-circuit ratio and phase-locked-loop parameters on the small-signal behavior of a VSC-HVDC converter," *IEEE Trans. Power Del.*, vol. 29, no. 5, pp. 2287–2296, Oct. 2014.

[11] B Huang *et al.*, "Study on subsynchronous oscillation in D-PMSGs-based wind farm integrated to power system," *IET Renewable Power. Gener.*, vol. 13, no. 1, pp. 16–26, 2019.

[12] Y. Xu, M. Zhang, L. Fan, and Z. Miao, "Small-signal stability analysis of type-4 wind in series-compensated networks," *IEEE Trans. Energy Convers.*, vol. 35, no. 1, pp. 529–538, Mar. 2020.

[13] V. Salis, A. Costabeber, S. M. Cox, P. Zanchetta, and A. Formentini, "Stability boundary analysis in single-phase grid-connected inverters with PLL by LTP theory," *IEEE Trans. Power Electron.*, vol. 33, no. 5, pp. 4023–4036, May 2018.

[14] L. Harnefors, M. Bongiorno, and S. Lundberg, "Input-admittance calculation and shaping for controlled voltage-source converters," *IEEE Trans. Ind. Electron.*, vol. 54, no. 6, pp. 3323–3334, Dec. 2007.

[15] B. Wen, D. Dong, D. Boroyevich, R. Burgos, P. Mattavelli, and Z. Shen, "Impedance-based analysis of grid-synchronization stability for three-phase paralleled converters," *IEEE Trans. Power Electron.*, vol. 31, no. 1, pp. 26–38, Jan. 2016.

[16] B. Wen, D. Boroyevich, R. Burgos, P. Mattavelli, and Z. Shen, "Analysis of D-Q small-signal impedance of grid-tied inverters," *IEEE Trans. Power Electron.*, vol. 31, no. 1, pp. 675–687, Jan. 2016.

[17] L. Fan and Z. Miao, "Nyquist-stability-criterion-based SSR explanation for type-3 wind generators," *IEEE Trans. Energy Convers.*, vol. 27, no. 3, pp. 807–809, Sep. 2012.

[18] K. Sun, W. Yao, J. Fang, X. Ai, J. Wen, and S. Cheng, "Impedance modeling and stability analysis of grid-connected DFIG-based wind farm with a VSC-HVDC," *IEEE J. Em. Sel. Top. P.*, vol. 8, no. 2, pp. 1375–1390, Jun. 2020.
[19] F. P. Demello and C. Concordia, "Concepts of synchronous machine stability as affected by excitation control," *IEEE Trans. Power App. Syst.*, vol. PAS-88, no. 4, pp. 316–329, Apr. 1969.
[20] E. V. Larsen and D. A. Swann, "Applying power system stabilizers, part I-III," *IEEE Trans. Power App. Syst.*, vol. PAS-100, no. 6, pp. 3017–3046, Jun. 1981.
[21] J. Liu *et al.*, "Impact of power grid strength and PLL parameters on stability of grid-connected DFIG wind farm," *IEEE Trans. Sustain. Energy*, vol. 11, no. 1, pp. 545–557, Jan. 2020.
[22] J. Hu, Q. Hu, B. Wang, H. Tang, and Y. Chi, "Small signal instability of PLL-Synchronized type-4 wind turbines connected to high-impedance AC grid during LVRT," *IEEE Trans. Energy Convers.*, vol. 31, no. 4, pp. 1676–1687, Dec. 2016.
[23] X. Wang, Y. Jun, J. Pei, P. Sun, and H. Zhang, "Analysis and damping control of small-signal oscillations for VSC connected to weak AC grid during LVRT," *IEEE Trans. Energy Convers.*, vol. 34, no. 3, pp. 1667–1676, Dec. 2019.

Xiaofang Wu received the B.S. degree in electrical engineering from Chongqing University, Chongqing, China, in 2017. She is currently working toward the Ph.D. degree with Xi'an Jiaotong University, Xi'an, China. Her research interests include power system stability and stability analysis of renewable energy grid connection system.

Zhengchun Du (Senior Member, IEEE) was born in Shaanxi, China, in 1963. He received the B.S., M.S., and Ph.D. degrees in electrical engineering from Xi'an Jiaotong University, Xi'an, China, in 1983, 1986, and 1993, respectively. He is currently a Professor of electrical engineering with Xi'an Jiaotong University. His research focuses on power system stability and control.

Yujun Li (Member, IEEE) received the B.Sc. degree in electrical engineering from Xi'an Jiaotong University, Xi'an, China, in 2011, the M.Sc. degree in electrical engineering from Zhejiang University, Hangzhou, China, in 2014, and the Ph.D. degree in electrical engineering from Hong Kong Polytechnic University, Hong Kong, in 2017. In 2017, he joined the School of Electrical Engineering, Xi'an Jiaotong University, where he was a Lecturer and is currently an Associate Professor with the School of Electrical Engineering. His main research interests include grid integration of renewable energy and high-voltage directing current modeling, fault analysis and detection of power systems.

Xiaotian Yuan (Graduate Student Member, IEEE) received the B.S. degree in electrical engineering in 2017 from Xi'an Jiaotong University, Xi'an, China, where he is currently working toward the Ph.D. degree. Since 2021, he has been a joint Ph.D. student funded by the China Scholarship Council, Nanyang Technological University, Singapore. His research interests include power system stability and control, grid-forming controls, and sub-synchronous oscillation analysis and mitigation.